PNAS RESEARCH ARTICLE | MICROBIOLOGY OPEN ACCESS

A common vesicle proteome drives fungal biofilm development

Robert Zarnowski[a,b], Hiram Sanchez[a,b], Anna Jaromin[c], Urszula J. Zarnowska[a,b], Jeniel E. Nett[a,b], Aaron P. Mitchell[c,d,1], and David Andes[a,b,1]

Edited by Joseph Heitman, Duke University School of Medicine, Durham, NC; received July 8, 2022; accepted August 1, 2022

Extracellular vesicles mediate community interactions among cells ranging from unicellular microbes to complex vertebrates. Extracellular vesicles of the fungal pathogen *Candida albicans* are vital for biofilm communities to produce matrix, which confers environmental protection and modulates community dispersion. Infections are increasingly due to diverse *Candida* species, such as the emerging pathogen *Candida auris*, as well as mixed *Candida* communities. Here, we define the composition and function of biofilm-associated vesicles among five species across the *Candida* genus. We find similarities in vesicle size and release over the biofilm lifespan. Whereas overall cargo proteomes differ dramatically among species, a group of 36 common proteins is enriched for orthologs of *C. albicans* biofilm mediators. To understand the function of this set of proteins, we asked whether mutants in select components were important for key biofilm processes, including drug tolerance and dispersion. We found that the majority of these cargo components impact one or both biofilm processes across all five species. Exogenous delivery of wild-type vesicle cargo returned mutant phenotypes toward wild type. To assess the impact of vesicle cargo on interspecies interactions, we performed cross-species vesicle addition and observed functional complementation for both biofilm phenotypes. We explored the biologic relevance of this cross-species biofilm interaction in mixed species and mutant studies examining the drug-resistance phenotype. We found a majority of biofilm interactions among species restored the community's wild-type behavior. Our studies indicate that vesicles influence the development of protective monomicrobial and mixed microbial biofilm communities.

vesicles | interspecies | *Candida* | biofilm | symbiosis

Significance

Candida species are commensal organisms commonly interacting in the same host niche. In the pathogenic state, they frequently grow as a biofilm, often in mixed infections. The present studies observe a reliance upon common extracellular vesicle cargo for biofilm structure and function supporting interactions among species. The results reveal a vesicle cargo-driven coordination among *Candida* species during biofilm formation.

Extracellular vesicles facilitate cell-to-cell communication via delivery of a complex protein, nucleic acid, carbohydrate, and lipid cargo (1–3). The importance of this form of cell signaling has been demonstrated across all taxonomic domains, from prokaryotic microbes to plants and animals (1, 2, 4–14). This form of transport of biologically active molecules has a pivotal role in a wide range of functions. In the context of microbial pathogens, vesicle effectors have shown to exert change within a microbial species as well as between the microbe and host (4, 6, 8, 9, 15–19). Specific vesicle cargo varies with cellular locations and environmental cues (5, 16, 20, 21). However, the roles of most individual cargo content have largely remained an enigma due to the complexity of vesicle composition.

A prevalent community behavior for most microbes is the formation of structured biofilms (22–24). The dynamics of biofilm formation generally include a continuum of phases that begin with the adherence of cells to a substrate and each other, followed by cell growth and encasement in an extracellular matrix, culminating in dispersion of cells from mature communities (25–27). Here, we focus on biofilms formed by diverse *Candida* species (25, 28–30). Most biofilm studies have focused on *Candida albicans*, yet nearly half of *Candida* infections are caused by other species. Moreover, this non-*albicans* subset continues to grow, most recently with the emergence of *Candida auris* (31, 32). *Candida* spp. are common human commensals of the oral cavity and gastrointestinal tract, closely interacting with each other and commensal prokaryotes. In the setting of host immune modulation or dysbiosis, *Candida* spp. often cause disease by propagating in either monomicrobial or frequently as mixed-species biofilms (33–42).

The biofilm lifestyle for *C. albicans* represents a highly dynamic process that is accompanied by variation of fungal extracellular vesicle sizes, quantities, and cargo across the developmental phases. In recent work, we defined a set of biofilm-distinct vesicle cargo proteins critical for key biofilm community functions (43). With that work as backdrop, we have asked here whether this biofilm vesicle cargo identity and function is conserved among *Candida* spp. and whether specific vesicle cargo proteins may drive interspecies community interaction. We find a set of common cargo proteins shared among *Candida* spp. biofilm vesicles that function interchangeably in biofilm drug tolerance and dispersion. This vesicle proteome thus endows *Candida* spp. communities with common properties that are central to biofilm pathogenicity.

Author affiliations: [a]Department of Medicine, University of Wisconsin, Madison, WI; [b]Department of Medical Microbiology and Immunology, University of Wisconsin, Madison, WI; [c]Department of Lipids and Liposomes, University of Wroclaw, Wrocław, Poland; and [d]Department of Microbiology, University of Georgia, Athens, GA

Author contributions: R.Z. and D.A. designed research; R.Z., H.S., A.J., and U.J.Z. performed research; R.Z., H.S., A.J., U.J.Z., J.E.N., A.P.M., and D.A. analyzed data; and R.Z., J.E.N., A.P.M., and D.A. wrote the paper.

The authors declare no competing interest.

This article is a PNAS Direct Submission.

[1]To whom correspondence may be addressed. Email: dra@medicine.wisc.edu or Aaron.Mitchell@uga.edu.

This article contains supporting information online at http://www.pnas.org/lookup/suppl/doi:10.1073/pnas.2211424119/-/DCSupplemental.

Published September 12, 2022.

Results

Diverse *Candida* spp. Produce Similar Extracellular Vesicles during Biofilm Growth. The characteristics of vesicles produced by *C. albicans* vary by the organism's mode of growth (16, 44). Recent examination of *C. albicans* during biofilm formation demonstrated a preponderance of smaller (exosome-like) vesicles that increased in No. as the biofilm matured and developed an extracellular matrix (16). To assess vesicle production by other *Candida* spp., we selected a representative isolate for commonly encountered *Candida* spp., including *Candida tropicalis*, *Candida parapsilosis*, *Candida glabrata*, and *C. auris*. All strains formed multilayer biofilms with extracellular matrix, but some variable architecture was observed among the strains (Fig. 1*A*). As shown previously, *C. tropicalis* produces biofilms with elongated hyphal cells, similar to *C. albicans*, while the other biofilms were composed of yeast only (36, 45, 46). Despite the different architectures, high-magnification imaging revealed vesicle-sized spheres decorating the surface of all the biofilms (Fig. 1*A*). Cryogenic electron microscopy imaging of these extracellular spheres demonstrated lipid bilayer structures characteristic of extracellular vesicles (Fig. 1*B*). Size-distribution analysis revealed single populations of relatively smaller sized vesicles for each biofilm, consistent with previously described vesicles for *C. albicans* biofilms and distinct from the bimodal size distribution of vesicles produced by planktonically growing *Candida* (Fig. 1*C*) (16, 44). The size of these vesicles is consistent with exosomes, as has been described for *C. albicans* biofilms (43). Time course quantitative measurements during biofilm maturation demonstrated an increase in vesicle production over time, paralleling biofilm maturation (Fig. 1*D*). The absolute vesicle quantities were similar across species, with the exception of a lower No. observed for *C. tropicalis* biofilms.

Comparison of Vesicle Cargo Composition. Extracellular vesicles carry cargo, including proteins, nucleic acids, polysaccharides, and lipids, with the specific composition of these governed by the cell type and influenced by environmental conditions (1, 2). Prior investigations observed distinct cargo during *C. albicans* biofilm formation when compared with planktonic growth (16). Much of the protein and polysaccharide components in *C. albicans* vesicles mirrored the extracellular matrix content (16). To assess biofilm vesicle cargo across for *Candida* spp., we first compared vesicle proteomes (Fig. 2). Vesicle protein cargo presence and abundance varied markedly among species (Fig. 2 *A* and *B* and *SI Appendix*, Table S1 and Datasets S1–S4). However, the relative similarity among proteomes appeared to parallel phylogenetic relatedness. For example, *C. albicans* appeared most similar to the

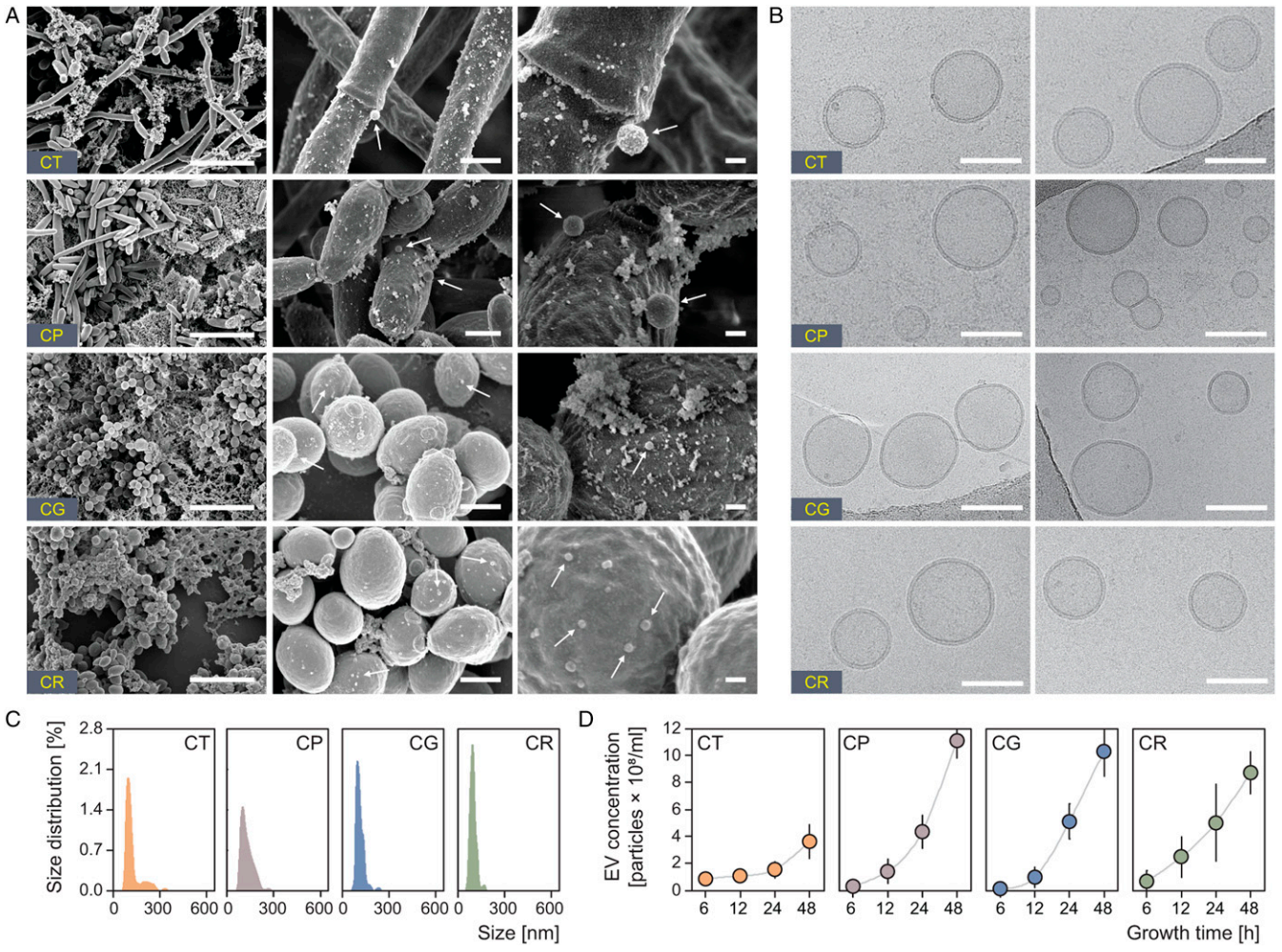

Fig. 1. Non-*albicans Candida* biofilms produce extracellular vesicles (EVs). (*A*) SEM of EV-like structures detected on the surface of *Candida* biofilm cells (large, medium, and small scale bars: 4 μm, 300 nm, and 100 nm, respectively). (*B*) Cryo-transition electron microscopy of *Candida* biofilm–derived EVs are about 100 nm in diameter and surrounded by a 7-nm-thick lipid bilayer (scale bar: 100 nm). (*C*) Size distribution of *Candida* biofilm EVs determined by nanoparticle tracking analysis (NTA); $n = 5$. (*D*) Quantitative analysis of EV concentration in *Candida* biofilms measured at various culture growth time points using NTA; $n = 5$. CT, *Candida tropicalis*; CP, *Candida parapsilosis*; CG, *Candida glabrata*; CR, *Candida auris*.

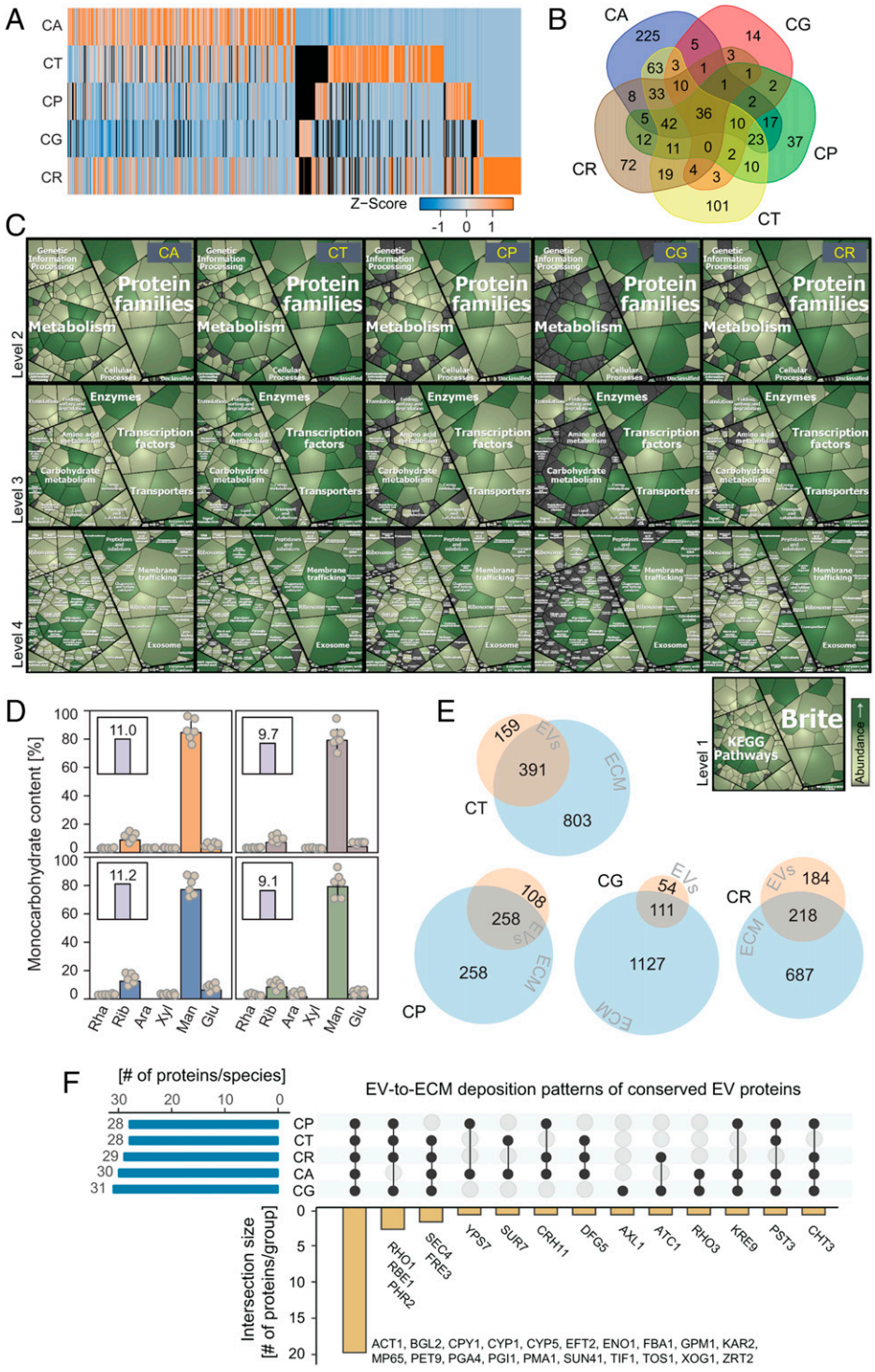

Fig. 2. Biochemical profiling of *Candida* biofilm extracellular vesicles. (*A*) A heatmap displaying differential expression of proteins found in the EV proteomes of *Candida* biofilms. Horizontal columns are colored according to the relative protein expression level of each protein. Jaffa bright orange and cerulean moderate blue indicate higher and lower expression Z scores, and black indicates missing proteins. The color intensity indicates the degree of protein up- or downregulation. Proteomic data were mapped using Heatmapper. (*B*) A Venn diagram depicting the qualitative profiling of *Candida* biofilm EV proteomes revealed the presence of 36 conserved common proteins. (*C*) KEGG/BRITE-based functional mapping of *Candida* EV proteomes. Clusters of low- to high-abundance biofilm EV proteins are shown in a color gradient ramp starting with light grayish yellow and reaching very dark desaturated lime green, while the very dark gray clusters depict missing proteins in a given proteome. Individual levels 4, 3, 2, and 1 represent identified proteins and are arranged inside higher-level regions according to their KEGG and BRITE functional category and pathway assignment by using a Voronoi treemap layout. (*D*) Gas chromatography–based monocarbohydrate profiling of *Candida* biofilm EVs; $n = 6$. Rha, rhamnose; Rib, ribose; Ara, arabinose; Xyl, xylose; Man, mannose; Glu, glucose. The inset ratios represent the mannan–glucan ratio, typical of the previously identified mannan–glucan complex. (*E*) The No. of exclusive (spindle powder blue and very soft orange) and common (grayish orange) proteins in corresponding *Candida* biofilm EVs and extracellular matrices (ECMs) illustrated by using a Venn diagram. CA, *Candida albicans*. (*F*) An upset plot demonstrating targeted sharing of conserved EV–cargo proteins in *Candida* biofilm extracellular matrices. Most of the conserved EV–cargo proteins are delivered via EVs into ECMs of five tested *Candida* biofilm–forming species. Black dots and lines show detected distribution patterns of conserved EV–cargo proteins in different *Candida* ECMs, while red bars reflect their frequencies. Inset: 78–86% of the conserved EV–cargo proteins end up deposited in the *Candida* ECM proteomes. Values reflect Nos. of the EV-to-ECM–deposited, EV-conserved proteins. Only one in the tested pool of 36 proteins, FLC2, was not detected in any of the biofilm ECMs.

closely related *C. tropicalis*, while the largest differences were found for *C. glabrata*, the most distant phylogenetic species (47). Despite these differences in proteomes, we identified a group of 36 proteins shared among all five species (Fig. 2*B* and Table 1). Several proteins of this group have been studied in *C. albicans* and have shown function in biofilm development, suggesting that vesicular trafficking may be involved in their activities (Fig. 2*C* and Table 1). For example, Bgl2 and Xog1 are glucanases critical for assembly of the extracellular matrix polysaccharides involved in antifungal drug sequestration and drug tolerance (48). Additional proteins in this set have also recently been shown to play key biofilm functions for *C. albicans*, including biofilm dispersion and drug tolerance, including Sun41, Cht3, Mp65, Tos1, and Zrt2 (16, 43). Despite the differences in specific vesicle proteome constituents observed among the species, representative inferred functional groups were largely congruent (Fig. 2*C*). Carbohydrate metabolism, glycan modification, and exosome biology were among the most common functional categories observed (*SI Appendix*, Table S1). This suggests that similar biological functions are required for biofilm growth but that the recruitment of machinery for these processes varies among species.

For *C. albicans* biofilms, vesicles contain the cargo required for assembly of biofilm extracellular matrix, including mannan and glucan (49, 50). We assessed the carbohydrate components of vesicles produced by non-*albicans Candida* biofilms and found them to be nearly identical by monosaccharide analysis (Fig. 2*D*). The ratios of mannan to glucan in the vesicles were compatible with the ratios required for assembly of the matrix mannan–glucan complex that is critical for drug tolerance, suggesting that vesicle delivery of these building blocks is conserved across species (Fig. 4*D*) (49, 50). We also considered whether non-*albicans* vesicle cargo proteomes similarly shared members with their corresponding matrix proteome. We detected variably shared matrix proteome contents among the species, ranging from 50% for *C. parapsilosis* (which is a percentage similar to *C. albicans*) to just under 10% for *C. glabrata* (Fig. 2*E*). Among the common vesicle proteomes, all but one protein was also identified as an extracellular matrix component (Fig. 2*F*). The carbohydrate and proteome similarities between vesicles and matrix for these species are consistent with vesicle delivery of the polysaccharides and at least a portion of proteins that construct this community protective shield.

Common *Candida* Vesicle Proteins Provide Multiple and Similar Biofilm Functions. *C. albicans* releases vesicles during biofilm growth, which deliver extracellular matrix components, promote drug tolerance, and impact cell dissemination (43). Individual vesicle cargo proteins have been shown to modulate these critical biofilm activities. We hypothesized that functional vesicle proteins required for key biofilm processes may be conserved across *Candida* spp. To assess this, we selected five candidate proteins—Cht3, Mp65, Sun41, Tos1, and Zrt2—for study based on their presence in biofilm vesicles across species and their recently described importance for *C. albicans* biofilm biology (43). We constructed deletion mutants in each species and examined the impact of gene disruption on drug tolerance and cell dispersion from mature biofilms (Fig. 3 *A* and *B*). We observed significant changes in these biofilm phenotypes for each mutant and species. For example, the *tos1*Δ/Δ mutants exhibited enhanced antifungal susceptibility in *C. albicans* (43) and each of the non-*albicans* species. This biofilm protection phenomenon is linked in *C. albicans* to drug sequestration by the extracellular matrix and specifically the mannan–glucan complex (49, 50). We found significant matrix total and mannan–glucan polysaccharide defects in most of the non-*albicans* drug-susceptible vesicle cargo mutants, consistent with a conserved mechanism across species (*SI Appendix*, Fig. S1) (45). Similarly, increases in biofilm dispersion were observed across species for the *cht3*Δ/Δ and *mp65*Δ/Δ mutants, respectively. Complementation restored a wild-type phenotype, providing genetic validation (Fig. 3 *A* and *B*). The clinical relevance of the drug tolerance was explored with an in vivo biofilm infection model for two proteins with prominent cross-species phenotypes (Fig. 3*C*) (51). We utilized the rat central venous catheter model to assess biofilm survival after antifungal therapy with the commonly used triazole, fluconazole. While wild-type biofilms were unresponsive to therapy, the cargo mutant biofilms exhibited marked treatment susceptibility. These results indicate that cargo proteins of all five *Candida* species contribute to biofilm drug insensitivity in vitro and in vivo.

Role of Vesicle Cargo in Biofilm Species Interactions. Does the core vesicle proteome exert biological function from its presence in vesicles or is vesicle localization coincidental? And do vesicles promote interspecies cooperation through this common proteome? To address these questions, we performed "add-back" studies to see whether wild-type vesicles could relieve mutant defects (16, 43). We combined wild-type vesicles collected from one species with mutant biofilms of each of the five species across a range of dosages. For each biofilm process, we selected a representative gene disruption that displayed a prominent phenotype across species.

Within species, exogenous wild-type vesicles reversed each mutant biofilm phenotype toward wild type, suggesting that disruption of the cargo protein was responsible for the phenotypes (Fig. 4 *A*–*D*). Exogenous vesicle addition did not completely reverse the mutant phenotypes, indicating the gene products may also function separately of vesicle cargo delivery. However, the findings demonstrate that the vesicles deliver functional biofilm cargo.

The addition of wild-type vesicles from one species to mutants of other species revealed considerable functional interchangeability (Fig. 4 *A*–*D*). For both the drug tolerance and dispersion phenotypes, the addition of wild-type vesicles to cargo mutant biofilms across species altered the phenotype toward the direction of wild type for all but two cross-species combinations. The exceptions were for the dispersion phenotype of the *C. albicans* mutant biofilm upon addition of *C. glabrata* and *C. auris* vesicles. However, without exception, the dose–response data found the vesicle concentration needed for maximal effect was considerably lower for within-species effects than for across-species effects (Fig. 4 *A* and *B* and *SI Appendix*, Figs. S2 and S3). These findings suggest these common vesicle proteins display interspecies functionality but exhibit more potent activity when presented within species. However, even the larger vesicle concentrations required for cross-species function are well within the physiologic range observed in time course vesicle production experiments (Fig. 1*D*).

To further explore the impact of cross-species vesicle interactions in the context of multiple species infection, we carried out mixed-species biofilm assays using mutants in different genes. We selected specific mutants ($TOS1^{-/-}$ and $CHT3^{-/-}$) in species for which antifungal susceptibility was found in many of the monospecies biofilms. We reasoned the vesicles from TOS1 deletion mutants would contain Cht3 protein and conversely vesicles from the CHT3 mutant would contain Tos1 protein, albeit from different *Candida* species. If the vesicles from distinct species were functional in a mixed biofilm, the community behavior would return to the drug-resistant state observed in wild-type strains. Compared with the

Table 1. Common cross-species EV proteome cargo during *Candida* spp. biofilm growth

Gene name	Description	Orthologous genes in *Candida* species				
		C. albicans	*C. tropicalis*	*C. parapsilosis*	*C. glabrata*	*C. auris*
ACT1	Actin	C1_13700W_A	CTRG1_03626	CPAR2_201570	CAGL0K12694g	B9J08_000486
ATC1	Cell wall acid trehalase ATC1 (EC 3.2.1.28) (Alpha,alpha-trehalase) (Alpha,alpha-trehalose glucohydrolase)	C1_06940C_A	CTRG1_04193	CPAR2_208980	CAGL0K05137g	B9J08_003397
AXL2	Axl2p	C4_04170C_A	CTRG1_05740	CPAR2_402930	CAGL0L08294g	B9J08_005205
BGL2	Glucan 1,3-beta-glucosidase BGL2 (EC 3.2.1.58) (Exo-1,3-beta-glucanase)	C4_02250C_A	CTRG1_00169	CPAR2_401600	CAGL0G00220g	B9J08_001418
CHT3	Chitinase 3 (EC 3.2.1.14)	CR_10110W_A	CTRG1_05827	CPAR2_200660	CAGL0M09779g	B9J08_002761
CPY1	Carboxypeptidase (EC 3.4.16.-)	C7_03360W_A	CTRG1_05137	CPAR2_703710	CAGL0M13651g	B9J08_003793
CRH11	Extracellular glycosidase CRH11 (EC 3.2.-.-) (Congo red hypersensitive protein 11)	C4_02900C_A	CTRG1_00263	CPAR2_400860	CAGL0G09449g	B9J08_004410
CYP1	Peptidyl-prolyl cis-trans isomerase (PPIase) (EC 5.2.1.8) (Cyclophilin) (CPH) (Cyclosporin A-binding protein) (Rotamase)	C7_02380C_A	CTRG1_05018	CPAR2_702740	CAGL0E01177g	B9J08_002142
CYP5	Peptidyl-prolyl cis-trans isomerase (PPIase) (EC 5.2.1.8) (Fragment)	C3_06360C_A	CTRG1_02246	CPAR2_404810	CAGL0H01529g	B9J08_000648
DFG5	Mannan endo-1,6-alpha-mannosidase DFG5 (EC 3.2.1.101) (Endo-alpha-1->6-D-mannanase DFG5)	C2_00520W_A	CTRG1_01122	CPAR2_213260	CAGL0M05049g	B9J08_002188
EFT2	Elongation factor 2 (EF-2)	C2_03100W_A	CTRG1_01315	CPAR2_211630	CAGL0A03234g	B9J08_002772
ENO1	Enolase 1 (EC 4.2.1.11) (2-phospho-D-glycerate hydro-lyase) (2-phosphoglycerate dehydratase)	C1_08500C_A	CTRG1_03163	CPAR2_207210	CAGL0F08261g	B9J08_000274
FBA1	Fructose-bisphosphate aldolase (FBP aldolase) (FBPA) (EC 4.1.2.13) (37 kDa major allergen) (Fructose-1, 6-bisphosphate aldolase) (IgE-binding allergen)	C4_01750C_A	CTRG1_00211	CPAR2_401230	CAGL0L02497g	B9J08_005239
FLC2	Flavin adenine dinucleotide transporter	CR_07100W_A	CTRG1_03117	CPAR2_204300	CAGL0M12320g	B9J08_000473
FRP3	Putative ammonium permease	C2_06680W_A	CTRG1_01795	CPAR2_104450	CAGL0M03465g	B9J08_002831
GPM1	Phosphoglycerate mutase (PGAM) (EC 5.4.2.11) (BPG-dependent PGAM) (MPGM) (Phosphoglyceromutase)	C2_03270W_A	CTRG1_01175	CPAR2_211810	CAGL0E06358g	B9J08_004375
KAR2	Hsp70 family ATPase	C2_01120W_A	CTRG1_01299	CPAR2_213780	CAGL0D02948g	B9J08_002819
KRE9	Protein of beta-1,6-glucan biosynthesis	C3_04180W_A	CTRG1_02327	CPAR2_404060	CAGL0C00363g	B9J08_000049
MP65	Cell surface mannoprotein MP65 (EC 3.2.1.-) (Mannoprotein of 65 kDa) (Soluble cell wall protein 10)	C2_10030C_A	CTRG1_02093	CPAR2_407410	CAGL0M13805g	B9J08_003799
PET9	ADP/ATP carrier protein	C5_00590W_A	CTRG1_05268	CPAR2_303940	CAGL0F04213g	B9J08_000434
PGA4	1,3-beta-glucanosyltransferase PGA4 (EC 2.4.1.-) (GPI-anchored protein 4)	C5_05390C_A	CTRG1_06145	CPAR2_100110	CAGL0F01287g	B9J08_005245
PGI1	Glucose-6-phosphate isomerase (GPI) (EC 5.3.1.9) (Phosphoglucose isomerase) (PGI) (Phosphohexose isomerase) (PHI)	CR_06340C_A	CTRG1_00601	CPAR2_204880	CAGL0H05445g	B9J08_000808
PHR2	pH-responsive protein 2 (pH-regulated protein 2)	C1_00220W_A	CTRG1_04296	CPAR2_109660	CAGL0M13849g	B9J08_000384
PMA1	Plasma membrane ATPase (EC 7.1.2.1)	C3_00720W_A	CTRG1_05722	CPAR2_502950	CAGL0A00495g	B9J08_002855
PST3	Flavodoxin-like fold family protein	C3_00720W_A	CTRG1_00572	CPAR2_204160	CAGL0K11858g	B9J08_004839
RBE1	Repressed by EFG1 protein 1 (PRY family cell wall protein 2)	C1_14120C_A	CTRG1_03687	CPAR2_700650	CAGL0F05137g	B9J08_003314
RHO1	GTP-binding protein RHO1	CR_02860W_A	CTRG1_00817	CPAR2_800200	CAGL0I08459g	B9J08_003889
RHO3	Rho family GTPase	C2_05030C_A	CTRG1_01644	CPAR2_209990	CAGL0G08558g	B9J08_005030
SEC4	Ras-related protein SEC4	CR_01750C_A	CTRG1_00852	CPAR2_800840	CAGL0F02123g	B9J08_001177
SUN41	Secreted beta-glucosidase SUN41 (EC 3.2.1.-)	C6_00820W_A	CTRG1_02944	CPAR2_603090	CAGL0J09922g	B9J08_005359
SUR7	Protein SUR7	C6_01720C_A	CTRG1_02860	CPAR2_602600	CAGL0L01551g	B9J08_005380
TIF1	ATP-dependent RNA helicase eIF4A (EC 3.6.4.13) (Eukaryotic initiation factor 4A) (eIF-4A) (Translation initiation factor 1)	C1_01350C_A	CTRG1_04436	CPAR2_109150	CAGL0I04356g	B9J08_000996
TOS1	Protein similar to alpha agglutinin anchor subunit	C3_01550C_A	CTRG1_02154	CPAR2_503650	CAGL0M05599g	B9J08_001002
XOG1	Glucan 1,3-beta-glucosidase (EC 2.4.1.-) (EC 3.2.1.58) (Exo-1, 3-beta-glucanase)	C1_02990C_A	CTRG1_04334	CPAR2_106000	CAGL0I00484g	B9J08_003251
YPS7	Putative aspartic endopeptidase	C7_02300W_A	CTRG1_05014	CPAR2_702810	CAGL0A02431g	B9J08_002149
ZRT2	Low-affinity Zn(2+) transporter	C2_02590W_A	CTRG1_01372	CPAR2_210740	CAGL0M04301g	B9J08_003657

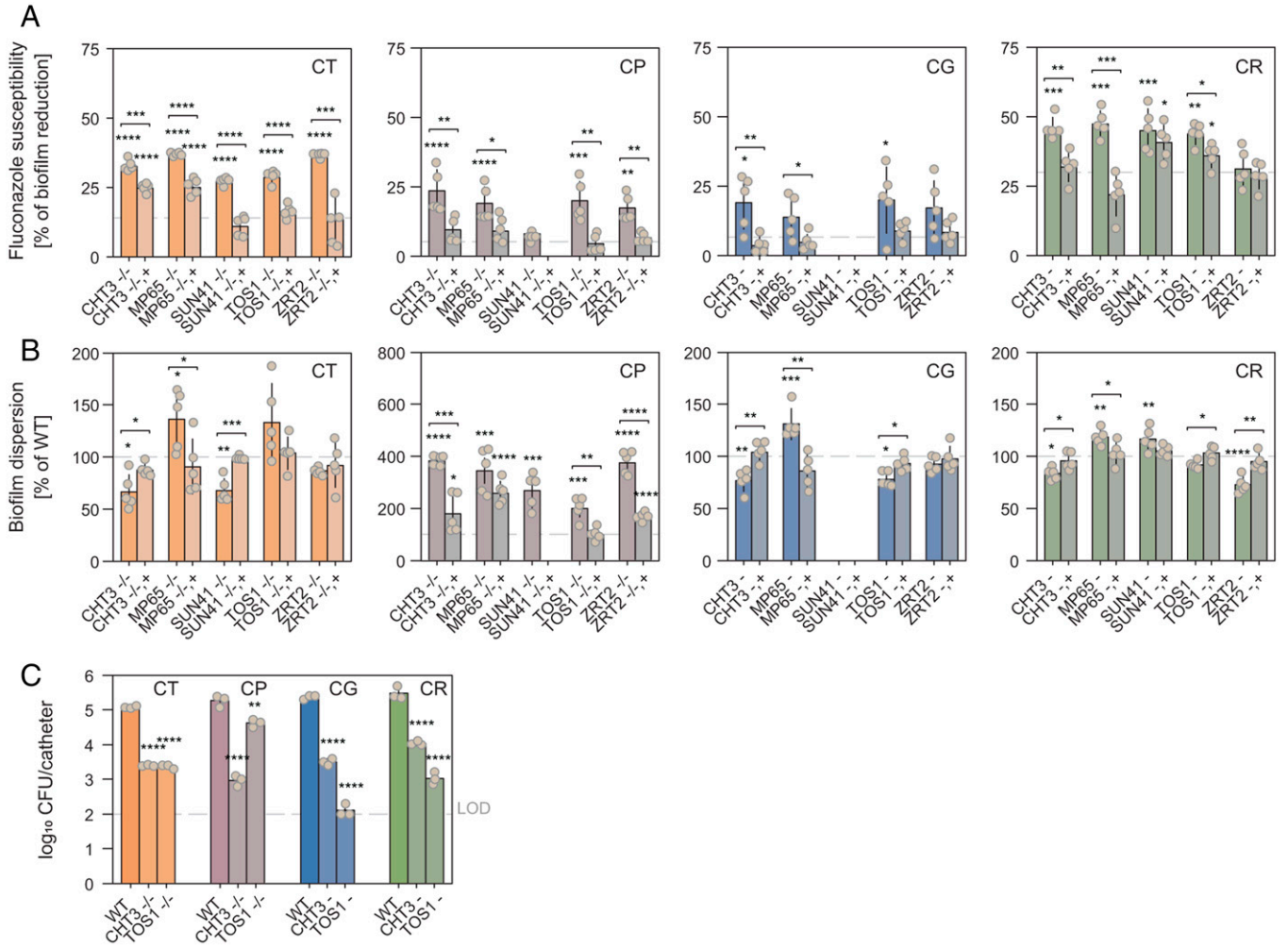

Fig. 3. Select conserved EV–cargo proteins modulate the biology of *Candida* biofilms. (*A*) The percent of reduction in *Candida* biofilm formation following treatment with 1,000 μg/mL fluconazole compared with untreated biofilms. The null deletions and corresponding complemented strains are shown for EV–cargo conserved proteins. Missing bars show mutant strains that could not be genetically created during this study. Each dot is an independent biological replicate. Data are presented as the mean ± SD; $n \geq 5$; *$P < 0.05$; **$P < 0.01$; ***$P < 0.005$*; ****$P \leq 0.0001$, using nonparametric Kruskal–Wallis one-way ANOVA with post hoc uncorrected Dunn's multiple comparison test. (*B*) The percent of fungal cell dispersion from mature *Candida* biofilms at 48 h. The null deletions and corresponding complemented strains are shown for EV–cargo conserved proteins. Missing bars show mutant strains that could not be genetically created during this study. Each dot is an independent biological replicate. Data are presented as the mean ± SD; $n \geq 5$; *$P < 0.05$; **$P < 0.01$; ***$P < 0.005$*; ****$P \leq 0.0001$, using nonparametric Kruskal–Wallis one-way ANOVA with post hoc uncorrected Dunn's multiple comparison test. WT, wild type. (*C*) Quantification of in vivo *Candida* biofilms following antifungal therapy using a rat venous catheter model. Select fluconazole-susceptible EV conserved protein cargo mutants were treated either with fluconazole 250 μg/mL or 0.9 M NaCl followed by the colony-forming unit (CFU) analysis. Each dot is an independent biological replicate. Data are presented as the mean ± SD; $n = 3$ animals and culture replicates per condition; ****$P \leq 0.0001$, using nonparametric Kruskal–Wallis one-way ANOVA with post hoc uncorrected Dunn's multiple comparison test. LOD, limit of detection.

enhanced drug susceptibility in individual species mutant biofilms, a majority (9 of 16) of the mixed species mutants had levels of resistance comparable to the wild-type strains (Fig. 4 *E* and *F*). The single exception was the combination of TOS1$^{-/-}$ mutants from *C. tropicalis*, which did not appear to behave in a cooperative fashion with other species CHT3$^{-/-}$ mutants. The reason for this difference is not clear. However, we speculate the relatively lower vesicle production by the *C. tropicalis* isolate utilized in these assays (Fig. 1*D*) may contribute to this observation. However, the aggregate data demonstrate that mixed-species biofilms with vesicle defects in specific protein content regain the ability to produce functional biofilms, consistent with cross-species vesicle functionality.

Discussion

The importance of extracellular vesicle release is widely recognized as an important means of cell interaction (1, 2, 4–7, 9–11, 14, 15, 52). Most studies of cargo content reveal a mixture of each macromolecular class (3). Investigations further demonstrate the vesicle cargo contents vary based on environmental conditions and spatial–temporal relationships (1, 12, 16, 20, 21, 44, 53). For example, vesicles produced by *C. albicans* growing in attached communities differ considerably from vesicles generated by the same species in free-floating conditions (16). Exploration of content among related cell types have also identified similarities and differences. For example, recent investigation of cargo in vesicles from different *Candida* species demonstrated large proteome differences (54, 55). The present studies focus upon biofilm growth of the five commonly encountered *Candida* species in this niche (25, 28–32, 36, 45, 56). Similar to other environment comparisons, we find marked differences in the biofilm vesicle proteome (12, 16, 20, 44, 54). It is interesting that the degree of variability within the biofilm niche appears to generally track with phylogenetic relatedness, with the *C. glabrata* and *C. auris* biofilm vesicle proteomes exhibiting the greatest variation from other species (47, 57). Despite these large differences, we did identify a

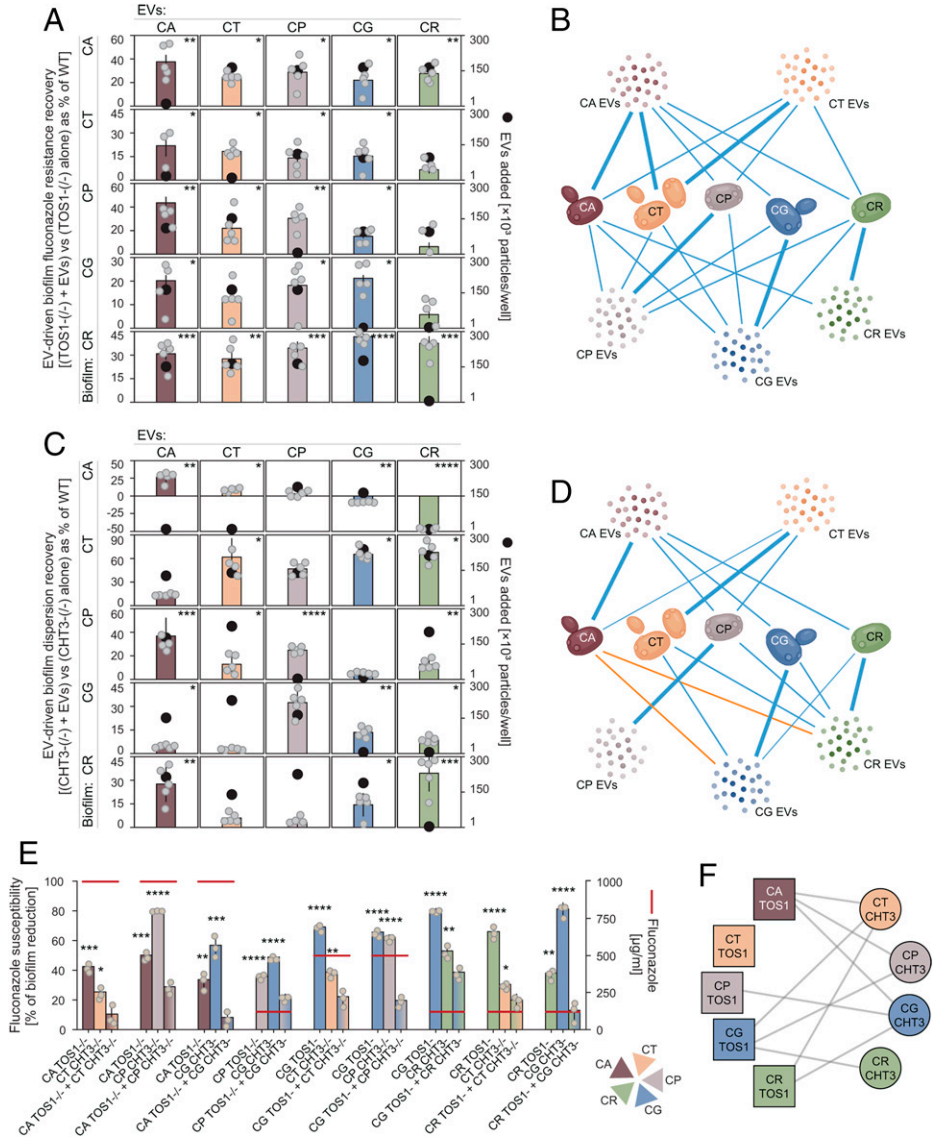

Fig. 4. Intra- and interspecies crosstalk between *Candida* biofilms occurs via EVs, which modulate biofilm biological properties and interactions. (*A*) Effects of exogenous *Candida* biofilm EVs on biofilm fluconazole susceptibility of TOS1 null mutants as measured by the 96-well XTT assay. Biofilm cultures of fluconazole-sensitive mutant strains (grouped in rows) were amended with WT EVs (columns) isolated from five different *Candida* species biofilm culture supernatants. *Candida* species color-coded bars indicate a phenotypic difference between a mutant biofilm grown with and without exogenous EVs expressed as % reduction of WT. Each gray dot is an independent biological replicate. Data are presented as the mean ± SD; $n = 5$; *$P < 0.05$; **$P < 0.01$; ***$P < 0.005$*; ****$P \leq 0.0001$, using nonparametric Kruskal–Wallis one-way ANOVA with post hoc uncorrected Dunn's multiple comparison test. Black dots indicate concentrations of exogenous EVs required for most optimal phenotypic response. (*B*) A network diagram illustrating an EV-driven crosstalk between *Candida* biofilms exposed to fluconazole. Only positive interactions (blue lines) between the tested *Candida* species and their EVs were detected, which resulted in regaining the *Candida* mature biofilms' ability to grow in the presence of fluconazole. The strength of the interaction is indicated by line thickness (thicker reflecting stronger effect than thinner lines). The strongest phenotypic recovery was observed when a biofilm of a given species was amended with its own species-specific EVs. Overall, this may indicate the presence of an evolutionary biocommunity-wide mechanism that provides an orchestrated response to xenobiotics. (*C*) Effects of exogenous *Candida* biofilm EVs on biofilm dispersion of CHT3 null mutants as measured by the 96-well XTT assay. Biofilm cultures of dispersion-dysregulated mutant strains (grouped in rows) were amended with WT EVs (columns) isolated from five different *Candida* species biofilm culture supernatants. *Candida* species color-coded bars indicate a phenotypic difference between a mutant biofilm grown with and without exogenous EVs expressed as % reduction of WT. Each gray dot is an independent biological replicate. Data are presented as the mean ± SD; $n = 5$; *$P < 0.05$; **$P < 0.01$; ***$P < 0.005$*; ****$P \leq 0.0001$, using nonparametric Kruskal–Wallis one-way ANOVA with post hoc uncorrected Dunn's multiple comparison test. Black dots indicate concentrations of exogenous EVs required for most optimal phenotypic response. (*D*) A network diagram summarizing an EV-driven intra- and interspecies regulation of dispersion in *Candida* biofilms. In general, positive (blue lines) interactions between the tested *Candida* species and their EVs were detected. The only negative interactions (orange line) were observed between CG/CR EVs and CA biofilms. The strongest phenotypic recovery was observed when a biofilm of a given species was amended with its own species-specific EVs. Overall, this may indicate the ability of mature *Candida* biofilms to take advantage of available *Candida* EVs and optimize biofilm maturation and dispersal. (*E*) Effect of mixed biofilm cultivation from different *Candida* species in CTH3 and TOS1 mutants on antifungal susceptibility. Nine of 16 susceptible cross-species biofilm interactions returned toward a WT drug-resistant phenotype. Each gray dot is an independent biological replicate. The fluconazole concentration used for the species interaction is represented by the red horizonal line. Data are presented as the mean ± SD; $n = 3$; *$P < 0.05$; **$P < 0.01$; ***$P < 0.005$*; ****$P \leq 0.0001$; comparison of single mutant biofilms to mixed biofilm data was performed using nonparametric Kruskal–Wallis one-way ANOVA with post hoc uncorrected Dunn's multiple comparison test. (*F*) A network diagram summarizing interactions among drug-susceptible *Candida* species mutants. Lines connecting individual species mutants indicate the interaction of the drug-susceptible mutants resulted in a return to WT (drug-resistance) in a mixed biofilm community. The absence of a connect line indicates the absence of an interacting drug-resistance phenotype.

common monosaccharide composition and a small set of similar proteins. It was not surprising to find resemblance in established vesicle markers, such as Hsp90 and Kar2 (2, 3, 58). Beyond these expected parallels, the putative ontology of protein similarities is intriguing, in that more than 40% of these components have been closely linked to important *C. albicans* biofilm functions via either expression or functional studies (Bgl2, Xog1, Sun41, Mp65, Cyp1, Cyp5, Cht3, Eno1, Fba1, Tos1, Frp3, Gpm1, Pgi1, Phr2, and Zrt2) (43, 48, 59–62). We were also interested to find the function of a quarter of the shared vesicle cargo is linked to the mannan–glucan complex constituents, which have been shown important for both biofilm-associated drug tolerance and dispersion (Bgl2, Xog1, Sun41, Chr11, Dfg5, Kre9, Mp65, Pga4, and Rho1) (43, 48, 63–65). Both findings indicate that there is conservation of functional vesicle cargo across species.

The focus of the current investigation is in the context of biofilm formation (23–25). Despite morphological differences among *Candida* species biofilms, the process for each proceeds through phases of maturation, requiring adhesion, production of a protective extracellular matrix, and dissemination from established biofilms to produce disease in distant organs (25, 27, 36, 45, 46, 66). We postulate vesicles provide similar functions in each species and that a core of vesicle effectors is responsible for these functions. This speculation was informed by the comparable structure and function of the biofilm extracellular matrix in these related fungal species (45, 50, 67). While few studies have considered vesicle cargo function in similar species, we were intrigued by the predominance of polysaccharide-modifying proteome components among the common *Candida* species components. Interestingly, study of wine yeast vesicle proteomes identified a single congruency in a polysaccharide-modifying glucanase (68). On this basis, it seemed logical to focus upon the role of proteomic similarities. In addition, the potential for conservation in function across species was informed by the previous demonstration of multifunctional cargo components in *C. albicans*, supporting a preservation of energy in these shared goods (43). We selected a subset of genes with prominent and multiple biofilm phenotypes in *C. albicans* to explore these hypotheses. We were excited to find these cargo components most often shared function in the four additional *Candida* species. Importantly, both the genetic and wild-type complementation assays indicate the functional specificity of these common cargo. The recent discovery of a promising antifungal inhibitor of vesicle delivery underscores the value of defining additional pathway components of importance for future drug-target discovery efforts (69).

Extracellular vesicles deliver cargo to coordinate interactions among cells in a variety of environments. The communication may occur between cells of similar or disparate species or even domains of life. In the microbial framework, bidirectional interactions have been described between microbes, as well as between a microbe and its host, often modulating the outcome of a pathogenic interplay (4, 6, 9–15, 17, 52, 70). An illustration of intercellular vesicle signaling within a microbial species was recently demonstrated for *Paracoccidioides brasiliensis*, where vesicle exposure modulated the response to endoplasmic reticulum stress induced by tunicamycin treatment (6). There are a No. of compelling examples of vesicle influence in signaling between a microbe and host. For instance, microRNA (miRNA) in vesicles released by the fungus, *Beauveria bassiana*, was found to target mosquito Toll receptor ligands, reducing immune protection (8). Conversely, host vesicles from the plant species, *Arabidopsis*, have been implicated in fungal virulence silencing in the *Botrytis cinerea* plant fungal pathogen (9). Monophyletic vesicle exchange among microbes has been described in the setting of biofilm communities (5, 6, 14–16, 43). However, the importance of multispecies biofilms in both environmental and medical settings is increasingly recognized (13, 22, 33–35, 37, 38, 71). These mixed genus microbial communities include both relationships among related species as well as those crossing kingdoms (72). Yet studies have most often not identified specific vesicle components utilized for these cross-species interchanges.

Candida species are among those microbes exhibiting a wide range of microbial interactions in both pathogenic and nonpathogenic or commensal environments (28, 33, 34, 37, 73). Microbiome studies that include fungal assessments regularly identify a mixture of *Candida* species (38, 39, 74, 75). Similarly, epidemiologic investigations commonly describe *Candida* infections involving more than a single *Candida* species (40–42). Thus, the ability of *Candida* species to utilize vesicle content to signal to a wide range of cell types would seem ideal for thriving in these multispecies environments. The present studies identified a subset of vesicle cargo commonalities shared among the most frequently observed human *Candida* pathogens. We discover the vesicles from one *Candida* species are capable of providing function to other *Candida* species via complementary assays, including the exogenous administration of cross-species vesicles as well as the sharing of vesicles across species in biologically relevant mixed-species biofilm mutant assays. The vesicle communication pathway delineated in the present investigations may in part explain the clinical observation of additional recalcitrance of mixed biofilm compared with monomicrobic infections (40, 42). This is maybe not surprising, considering the conservation of extracellular vesicle pathways among eukaryotes (2, 53). However, the impact of vesicles on biofilm processes was consistently greater for within-species studies than for cross-species interactions, suggesting a component of species specificity. Similar to comparison of structural vesicle components among species, there is a suggestion that the ability of species to offer function across species is evolutionarily driven. For example, the capacity of vesicles and cargo mutants from the more phylogenetically distant *C. auris* species to complement biofilm dispersion function for the more closely related species was limited or absent. Finding both conservation and divergence of vesicle function in an evolutionary context is reminiscent of the role and targets of transcription factors in *Candida spp.* biology (76, 77). Further understanding the chemical biology of these symbiotic microbial interactions is critical for design of therapeutics to impact biofilm formation.

Materials and Methods

Culture Media and Conditions. Stocks of *Candida* strains were stored in 15% glycerol frozen at −80 °C and routinely maintained on YPD agar plates (1% yeast extract, 2% Bacto peptone, 2% dextrose, and 2% Bacto agar). Liquid cultures were grown in broth YPD (1% yeast extract, 2% Bacto peptone, and 2% dextrose) rotating at 200 rpm at 30 °C. For biofilm assays, strains were cultured in filter-sterilized Roswell Park Memorial Institute medium 1640 (RPMI), buffered with 4-morpholinepropanesulfonic acid (MOPS) and pH adjusted to 7.0 (78).

Fungal Mutant Construction Strategies. Strains used in this study along with their genotypes are listed in *SI Appendix*, Table S2. The parental strains *C. tropicalis* CAY3764, *C. parapsilosis* CPL2H1, *C. glabrata* HTL, and *C. auris* B11804 (wild-type Colombian isolate of the South American clade IV) were used to generate homozygous deletion mutants using available auxotrophic and drug resistance marker–based strategies (79–81). Gene-replacement cassettes were

prepared using a PCR-assisted gene splicing by overlap extension DNA assembly procedure (82). At least two independent mutants were created for each gene of interest. Gene deletion complementation with a single wild-type gene copy and an antibiotic-resistance marker was done either with nourseothricin in case of *C. tropicalis* and *C. parapsilosis* or with hygromycin B in case of *C. glabrata* and *C. auris*, respectively. Correct integration sites during gene deletion and complementation procedures were confirmed by routine PCR. The primers utilized for strain construction and genetic manipulations are listed in *SI Appendix*, Table S3.

Large-Scale Biofilm Cultures and Extracellular Matrix and Extracellular Vesicle Isolation. *Candida* biofilms were grown using a large-scale rolling bottle biofilm model system (83). Culture media were carefully decanted from the polystyrene bottles after 24 and 48 h of incubation at 37 °C. The remaining fungal biomass was dislodged from the roller bottle surface with a sterile spatula and used to isolate the extracellular matrix. The intact biofilms were then gently subjected to sonication to remove matrix from fungal cells. Sonication with done with a 6-mm microtip head at 20 kHz with an amplitude of 30% for 8 min, followed by centrifugation to separate the biomass from the matrix and filter sterilization, and the isolated matrix was then lyophilized. Culture supernatants were filter sterilized and concentrated down to about 25 mL using a Vivaflow 200 unit (Sartorius AG) equipped with a Hydrosart 30-kDa cutoff membrane. Samples were centrifuged in order to remove smaller cellular debris particulates first at 10,000 × g for 1 h at 4 °C. The pellet was discarded, and the resulting supernatant was centrifuged again at 100,000 × g for 1.5 h at 4 °C. Next, the supernatant was discarded, and the pellet was then washed in 5 mL of phosphate-buffered saline (PBS) and recentrifuged at 100,000 × g for 1 h at 4 °C. The collected extracellular vesicles were next polished by flash size-exclusion chromatography on a qEV/35 nm column (Izon Science), filter sterilized, and stored until further use at 4 °C.

Intermediate-Scale Biofilm Cultures. Intermediate-scale biofilm cultures were grown in six-well polystyrene plates and were used to determine biofilm extracellular matrix carbohydrate composition in wild-type and mutant strains of all five *Candida* species. Biofilms were seeded with 10^6 yeast cells per well. The nonadherent cells were removed after a 60-min-long static adherence incubation, and 1 mL of fresh RPMI medium was applied to each well. The biofilms were grown on an orbital shaker set at 50 rpm at 37 °C for 24 h, then the medium was replaced with fresh RPMI and the incubation was continued for another 24 h. Biofilms were removed from wells with a sterile spatula and harvested in sterile water (1 mL/well). The aliquots were combined in a 15-mL Falcon tube, and the biofilm biomass was subjected to sonication in a water bath sonicator for 20 min. To separate the dissolved extracellular matrix (ECM) from fungal biomass, the sample was centrifuged at 2,880 × g at 4 °C for 20 min. Five milliliters of the collected ECM suspension was placed in a clear 8-mL glass screw thread vial and dried overnight at 60 °C. Such prepared samples were used for gas chromatography–based carbohydrate profiling as described below.

Biofilm Antifungal Drug Susceptibility Assay. Antifungal drug susceptibility of *Candida* biofilms was measured in 96-well, flat-bottom polystyrene plates. Biofilms were treated with fluconazole, one of the most prescribed antifungal azoles, at 1,000 mg/mL (84). For *C. albicans* and *C. tropicalis* cultures, the antifungal drug was applied twice, after 6 and 24 h of incubation. For *C. parapsilosis*, *C. glabrata*, and *C. auris* cultures, fluconazole was dosed only ones after 24 h. For mixed biofilm assays, the TOS1$^{-/-}$ and CHT3$^{-/-}$ mutants from each species were combined in equal concentrations at the time of inoculation. Antifungal drug susceptibility of mixed-species mutant biofilms was measured in 96-well, flat-bottom polystyrene plates. Fungal cell inocula (10^6 cells/mL) were prepared out of overnight yeast cultures in YPD at 30 °C. Fifty microliters of yeast cells per tested strain well were seeded and brought up to 100 μL with saline. Inocula of double-mutant combinations were premixed before biofilm seeding. Fluconazole was applied twice after 6 and 24 h in biofilms containing *C. albicans* and/or *C. tropicalis*, whereas biofilms consisting of *C. parapsilosis*, *C. glabrata*, or *C. auris* were treated with fluconazole once after 24 h of incubation. Biofilms were then evaluated using the colorimetric tetrazolium reduction XTT assay. To enhance XTT reduction, phenazine methosulfate (2 mM) was used as electron acceptor in *C. albicans* and *C. tropicalis* assays, whereas menadione (1 mM in acetone) was used in assays involving *C. parapsilosis*, *C. glabrata*, and *C. auris*. Mixed biofilms consisting of one of *C. albicans*/*C. tropicalis* and one of *C. parapsilosis*/*C. glabrata*/*C. auris* were seeded in duplicate, and separate XTT reactions with phenazine methosulfate or menadione were performed. Absorbance at 492 nm was measured using an automated Cytation 5 imaging reader (BioTek).

Biofilm-Dispersion Assay. Biofilm dispersion was determined in 96-well plates. Fungal cell inocula (10^6 cells/mL) were prepared out of overnight yeast cultures in YPD at 30 °C, followed by dilution in RPMI–MOPS based on count Nos. with an automated Countess II cell counter (Invitrogen). One hundred microliters of yeast cells per well were seeded, and the plates were incubated for 6 h at 37 °C, followed by gentle washing with PBS and fresh RPMI applied. After continued incubation for another 24 h, the biofilms were washed with PBS, and RPMI was replaced with fresh one and allowed to incubate for 24 h at 37 °C. Supernatants were then carefully removed from biofilm cultures, and 100-μL aliquots were transferred to a fresh 96-well plate. The amount of dispersed biofilm cells was determined by the described above-modified XTT assay, in which both XTT and N-methyl dibenzopyrazine methyl sulfate or menadione were applied at double concertation. Dispersion capacity of biofilms was calculated using the change in absorbance compared with that of controls.

Exogenous Extracellular Vesicle Addback Assays and Functional Network Construction. Biological impact of exogenous extracellular vesicles on *Candida* biofilm properties (susceptibility to fluconazole and dispersion) was determined in 96-well plates. Fungal cell inocula (10^6 cells/mL) were prepared out of overnight yeast cultures in YPD at 30 °C, followed by dilution in RPMI–MOPS based on count Nos. with an automated Countess II cell counter (Invitrogen). One hundred microliters of yeast cells per well were seeded. TOS1 deletion strains were used to evaluate biofilm susceptibility to fluconazole, whereas CHT3 deletion mutants were used in dispersion assays. Extracellular vesicles isolated from all five tested *Candida* species were used in combinations in biofilms of all five *Candida* species at normalized concentrations ranging between 1×10^4 and 3×10^6 particles/mL. For the biofilm antifungal susceptibility assay, exogenous extracellular vesicles were added after an initial 5-h biofilm formation period and incubated for an additional hour followed by the drug treatment as described above. Biofilm cultures were treated with fluconazole (1,000 μg/mL). For the biofilm-dispersion assay, exogenous extracellular vesicles were added after 24 h of growth. Biofilms' growth in cultures with and without exogenous extracellular vesicles was evaluated by the XTT assay as described above. The obtained phenotypic outcomes were organized into visual *Candida* biofilm phenotypic networks using the Cytoscape platform (85).

Time-Course Assessment of Extracellular Vesicle Production in Biofilms. Quantitative analysis of extracellular vesicles (EVs) produced in *Candida* biofilms was determined at various culture-growth time points in 96-well plates. Fungal cell inocula (10^6 cells/mL) were prepared out of overnight yeast cultures in YPD at 30 °C, followed by dilution in RPMI–MOPS based on count Nos. with an automated Countess II cell counter (Invitrogen). One hundred microliters of yeast cells per well were seeded and incubated for 6, 12, 24, and 48 h, followed by collection of supernatants, which were then filter sterilized and subjected to EV analysis as described below. Data were normalized based on XTT assay readouts as described above.

EV Analyses. Exosomes were quantified using nanoparticle-tracking analysis. Initial analyses were performed on a Zetasizer Nano-ZS (Malvern Instruments) (86). EV samples were diluted in PBS to a final volume of 1 mL and pretested to obtain an ideal 30–100 particles per frame rate using a NanoSight NS300 system (Malvern). The following settings were applied: camera level was increased to 16 and camera gain to 2 until tested images were optimized and nanoparticles were distinctly visible without exceeding particle signal saturation. Each measurement consisted of five 1-min videos with a delay of 5 s between sample introduction and the start of the first measurement. For detection-threshold analysis, the counts were limited to 10–100 red crosses and no more than five to seven blue crosses. Acquired data were analyzed using the NanoSight Software NTA 3.4 Build 3.4.003. At least 1,000 events in total were tracked per sample in order to minimize data skewing based on single large particles (87).

In Vivo *Candida* Catheter Model. *Candida* biofilm growth during infection of implanted medical devices was measured using an external jugular-vein, rat-catheter infection model (51). For drug-treatment experiments, fluconazole at a

concentration of 250 μg/mL was instilled and dwelled in the catheter over a 24-h period. The posttreatment viable burden of *Candida* biofilm on the catheter surface was compared with untreated control growth. Three replicates were performed for treatment and control conditions. Quantitative cultures of *Candida* spp. after 24 h of in vivo growth were utilized to measure viable biofilm cell burden.

Scanning Electron Microscopy of *Candida* Biofilms. The surface of *Candida* biofilms grown in 6-well plates was imaged using scanning electron microscopy (SEM) (45). Briefly, 40 μL of an inoculum of 10^8 cells/mL in RPMI was added to the coverslips and incubated at 37 °C for 60 min. One milliliter RPMI was added to each well, and the plates were incubated at 37 °C for 20 h. One milliliter fixative (4% formaldehyde and 1% glutaraldehyde in PBS) was then added to each well prior to incubation at 4 °C overnight. Coverslips were then washed with PBS prior to incubation in 1% OsO_4 for 30 min. Samples were then serially dehydrated in ethanol (30–100%). Critical point drying was used to completely dehydrate the samples prior to palladium–gold coating. Samples were imaged on a SEM LEO 1530, with Adobe Photoshop 2022 (v. 23.2.2) used for image compilation.

Cryo-electron Microscopy. Cryo-electron microscopy (cryo-EM) was done at the University of Wisconsin–Madison Cryo Research Center. CF200-CU grids (EMS) were glow discharged for 30 s at 15 mA with a chamber pressure of 0.004 mbar. Plunge freezing occurred in an FEI Vitrobot Mark IV cryoplunge freezing robot at 4 °C. Three microliters of sample was then spotted onto the grid, blotted for 5 s with a blotting pressure of 1, and plunge frozen into liquid ethane. Grids were transferred into liquid nitrogen for storage. cryo-EM imaging was performed on a Talos Arctica (ThermoScientific) at 200 kV. Images (defocus of −2 μm) were recorded on a post-GIF Gatan K3 camera in energy filtered transmission electron microscopy mode (3.7 Å/pixel at 24-kx magnification and 1.1 Å/pixel at 79-kx magnification) with a 20-eV slit, CDS counting mode, using SerialEM 3.8. Two magnifications were set for high-resolution imaging: 24-kx magnification (spot size 7, C2 aperture 100, C2 lens power 38.133%, objective aperture 100, pixel size 3.7Å) and 79-kx magnification (spot size 4, C2 aperture 70, C2 lens power 42.546%, objective aperture 100, pixel size 1.1Å). A total dose of 21.6 e-/Å2 at 24-kx magnification and 48 e-/Å2 at 79-kx magnification were used, respectively.

Gel-Free Proteomics. Enzymatic "in liquid" digestion and mass spectrometric analysis was done at the Mass Spectrometry Facility, Biotechnology Center, University of Wisconsin–Madison. Two hundred micrograms of proteins were extracted by precipitation with 15% trichloroacetic acid/60% acetone and then incubated at −20 °C for 30 min. The matrix or vesicle preparation was centrifuged at 16,000 × g for 10 min, and the resulting pellets were washed twice with ice-cold acetone, followed by an ice-cold MeOH wash. Pelleted proteins were resolubilized and denatured in 10 μL of 8 M urea in 100 mM NH_4HCO_3 for 10 min, then diluted to 60 μL for tryptic digestion with the following reagents: 3 μL of 25 mM dithiothreitol, 4.5 μL of acetonitrile, 36.2 μL of 25 mM NH_4HCO_3, 0.3 μL of 1M Tris·HCl, and 6 μL of 100 ng/μL Trypsin Gold solution in 25 mM NH_4HCO_3 (Promega). Digestion was conducted in two stages: first overnight at 37 °C and then additional 4 μL of trypsin solution were added and the mixture was incubated at 42 °C for an additional 2 h. The reaction was terminated by acidification with 2.5% trifluoroacetic acid to a final concentration of 0.3% and then centrifuged at 16,000 × g for 10 min. Trypsin-generated peptides were analyzed by nano-liquid chromatography–tandem mass spectrometry (nano-LC-MS/MS) using the Agilent 1100 nanoflow system (Agilent) connected to a hybrid linear ion trap–orbitrap mass spectrometer (LTQ-Orbitrap, Thermo Fisher Scientific) equipped with a nanoelectrospray ion source. Capillary high-performance LC (HPLC) was performed using an in-house fabricated column with an integrated electrospray emitter, as described elsewhere (88). Sample loading and desalting were achieved using a trapping column in line with the autosampler (Zorbax 300SB-C18, 5 μm, 5 × 0.3 mm, Agilent). The LTQ-Orbitrap was set to acquire MS/MS spectra in a data-dependent mode as follows: MS survey scans from 300 to 2,000 *m/z* were collected in profile mode with a resolving power of 100,000. MS/MS spectra were collected on the five most abundant signals in each survey scan. Dynamic exclusion was employed to increase the dynamic range and maximize peptide identifications. Raw MS/MS data were searched against a concatenated *C. albicans* amino acid sequence database using an in-house MASCOT search engine (89). Identified proteins were further annotated and filtered to 1.5% peptide and 0.1% protein false discovery rate with Scaffold Q+ version 4.10.0 (Proteome Software Inc.) using the protein prophet algorithm (90). Proteomic data were mapped using Heatmapper (91). The mass spectrometry proteomics data have been deposited to the ProteomeXchange Consortium via the proteomics identifications (PRIDE) partner repository with the dataset identifier PXD035068 and 10.6019/PXD035068 (92) (93).

Proteome Functional Mapping. The obtained Candida EV and matrix proteomes were analyzed using the Kyoto Encyclopedia of Genes and Genomes (KEGG) (94, 95). Both KEGG pathway maps and BRITE hierarchies databases were used. Each protein predicted from the *C. albicans* genome assigned a KEGG Ontology ID was obtained and the specific pathway and superpathway membership information retained. For non-*albicans Candida* species, Protein Basic Local Alignment Search Tool–based mapped protein orthologies and homologies among *Candida* species were obtained from the Candida Genome Database (96). This was then correlated with the experimental proteome data, and the No. of proteins expressed within a given pathway was then determined. Tabulated proteins were presented as a percentage out of the total No. of proteins predicted to belong to a given pathway from the *C. albicans* genome, as determined by KEGG/BRITE assignments. The visualization of relative quantities of biofilm proteins was done using KEGG/BRITE protein functional categorization (97). Based on this hierarchical classification scheme, Voronoi treemaps were constructed using Paver (v. 2.1.9, DECODON Software UG). This approach divides screen space according to hierarchy levels in which the main functional categories determine screen sections on the first level, subsidiary categories on the second level, and so forth. The polygonic cells of the deepest level represented functionally classified proteins and were colored according to relative abundance of each protein that was determined based on total counts of corresponding trypsin-digested peptides.

EV Carbohydrate Profiling. Carbohydrates in biofilm EVs were analyzed based on the modified procedures reported elsewhere (50). Monosugars were converted to alditol acetate derivatives (98) and then identified and quantified by gas chromatography on a Shimadzu GC-2010 system (Shimadzu). A Crossbond 50% cyanopropylmethyl/50% phenylmethyl polysiloxane column was used (15 m × 0.25 mm with 0.25-μm film thickness, RTX-225, Restek). The gas–liquid chromatography conditions were as follows: injector at 220 °C, flame ionization detector at 240 °C, and a temperature program of 215 °C for 2 min, then 4 °C/min up to 230 °C before holding for 11.25 min, run at constant linear velocity of 33.4 cm/s and split ratio of 50:1.

Statistics. Datasets of equal of different sample sizes were analyzed using the nonparametric Kruskal–Wallis one-way ANOVA with uncorrected Dunn's multiple comparisons without prior elimination of outliers. Data were processed with GraphPad Prism 9 for Windows 64-bit (version 9.3.1 [471]).

Ethics Statement. All animal procedures were approved by the Institutional Animal Care and Use Committee at the University of Wisconsin–Madison according to the guidelines of the Animal Welfare Act, The Institute of Laboratory Animal Resources Guide for the Care and Use of Laboratory Animals, and Public Health Service Policy. The approved animal protocol No. is DA0031.

Data, Materials, and Software Availability. The authors declare that the data supporting the findings of this study are available within *SI Appendix*. Source data are provided with this paper. The mass spectrometry proteomics data have been deposited to the ProteomeXchange Consortium via the PRIDE partner repository with the dataset identifier PXD035068 and 10.6019/PXD035068 (93).

All data are included in the manuscript and/or *SI Appendix*.

ACKNOWLEDGMENTS. D.A. and A.P.M. were funded by R01AI073289. We thank Jen Fossen for technical assistance.

1. L. Brown, J. M. Wolf, R. Prados-Rosales, A. Casadevall, Through the wall: Extracellular vesicles in Gram-positive bacteria, mycobacteria and fungi. *Nat. Rev. Microbiol.* **13**, 620–630 (2015).
2. E. R. Abels, X. O. Breakefield, Introduction to extracellular vesicles: Biogenesis, RNA cargo selection, content, release, and uptake. *Cell. Mol. Neurobiol.* **36**, 301–312 (2016).
3. M. P. Zaborowski, L. Balaj, X. O. Breakefield, C. P. Lai, Extracellular vesicles: Composition, biological relevance, and methods of study. *Bioscience* **65**, 783–797 (2015).
4. E. Bielska *et al.*, Pathogen-derived extracellular vesicles mediate virulence in the fatal human pathogen *Cryptococcus gattii*. *Nat. Commun.* **9**, 1556 (2018).
5. P. C. Albuquerque *et al.*, Vesicular transport in *Histoplasma capsulatum*: An effective mechanism for trans-cell wall transfer of proteins and lipids in ascomycetes. *Cell. Microbiol.* **10**, 1695–1710 (2008).
6. T. A. Bitencourt *et al.*, Fungal extracellular vesicles are involved in intraspecies intracellular communication. *MBio* **13**, e0327221 (2022).
7. C. Coelho *et al.*, *Listeria monocytogenes* virulence factors, including listeriolysin O, are secreted in biologically active extracellular vesicles. *J. Biol. Chem.* **294**, 1202–1217 (2019).
8. C. Cui *et al.*, A fungal pathogen deploys a small silencing RNA that attenuates mosquito immunity and facilitates infection. *Nat. Commun.* **10**, 4298 (2019).
9. Q. Cai *et al.*, Plants send small RNAs in extracellular vesicles to fungal pathogen to silence virulence genes. *Science* **360**, 1126–1129 (2018).
10. S. Moriano-Gutierrez *et al.*, The noncoding small RNA SsrA is released by *Vibrio fischeri* and modulates critical host responses. *PLoS Biol.* **18**, e3000934 (2020).
11. A. Ricciardi *et al.*, Extracellular vesicles released from the filarial parasite *Brugia malayi* downregulate the host mTOR pathway. *PLoS Negl. Trop. Dis.* **15**, e0008884 (2021).
12. G. Vargas *et al.*, Compositional and immunobiological analyses of extracellular vesicles released by *Candida albicans*. *Cell. Microbiol.* **17**, 389–407 (2015).
13. R. Wu, Y. Tao, Y. Cao, Y. Zhou, H. Lin, *Streptococcus mutans* membrane vesicles harboring glucosyltransferases augment *Candida albicans* biofilm development. *Front. Microbiol.* **11**, 581184 (2020).
14. J. Lin *et al.*, A Pseudomonas T6SS effector recruits PQS-containing outer membrane vesicles for iron acquisition. *Nat. Commun.* **8**, 14888 (2017).
15. D. Eliaz *et al.*, Exosome secretion affects social motility in *Trypanosoma brucei*. *PLoS Pathog.* **13**, e1006245 (2017).
16. R. Zarnowski *et al.*, *Candida albicans* biofilm-induced vesicles confer drug resistance through matrix biogenesis. *PLoS Biol.* **16**, e2006872 (2018).
17. R. Prados-Rosales *et al.*, Mycobacteria release active membrane vesicles that modulate immune responses in a TLR2-dependent manner in mice. *J. Clin. Invest.* **121**, 1471–1483 (2011).
18. L. D. Halder *et al.*, *Candida albicans* induces cross-kingdom miRNA trafficking in human monocytes to promote fungal growth. *MBio* **13**, e0356321 (2022).
19. V. K. A. Silva *et al.*, Replicative aging remodels the cell wall and is associated with increased intracellular trafficking in human pathogenic yeasts. *MBio* **13**, e0019022 (2022).
20. J. Karkowska-Kuleta *et al.*, Characteristics of extracellular vesicles released by the pathogenic yeast-like fungi *Candida glabrata*, *Candida parapsilosis* and *Candida tropicalis*. *Cells* **9**, E1722 (2020).
21. L. Matos Baltazar *et al.*, Antibody binding alters the characteristics and contents of extracellular vesicles released by *Histoplasma capsulatum*. *MSphere* **1**, e00085-15 (2016).
22. T. J. Battin, L. A. Kaplan, J. Denis Newbold, C. M. Hansen, Contributions of microbial biofilms to ecosystem processes in stream mesocosms. *Nature* **426**, 439–442 (2003).
23. J. W. Costerton, P. S. Stewart, E. P. Greenberg, Bacterial biofilms: A common cause of persistent infections. *Science* **284**, 1318–1322 (1999).
24. L. Hall-Stoodley, J. W. Costerton, P. Stoodley, Bacterial biofilms: From the natural environment to infectious diseases. *Nat. Rev. Microbiol.* **2**, 95–108 (2004).
25. J. Chandra *et al.*, Biofilm formation by the fungal pathogen *Candida albicans*: Development, architecture, and drug resistance. *J. Bacteriol.* **183**, 5385–5394 (2001).
26. H. C. Flemming, J. Wingender, The biofilm matrix. *Nat. Rev. Microbiol.* **8**, 623–633 (2010).
27. P. Uppuluri *et al.*, Dispersion as an important step in the *Candida albicans* biofilm developmental cycle. *PLoS Pathog.* **6**, e1000828 (2010).
28. M. A. Pfaller, D. J. Diekema, Epidemiology of invasive candidiasis: A persistent public health problem. *Clin. Microbiol. Rev.* **20**, 133–163 (2007).
29. E. M. Kojic, R. O. Darouiche, Candida infections of medical devices. *Clin. Microbiol. Rev.* **17**, 255–267 (2004).
30. P. G. Pappas *et al.*, Clinical practice guideline for the management of Candidiasis: 2016 update by the infectious diseases society of America. *Clin. Infect. Dis.* **62**, e1–e50 (2016).
31. A. Chowdhary, C. Sharma, J. F. Meis, *Candida auris*: A rapidly emerging cause of hospital-acquired multidrug-resistant fungal infections globally. *PLoS Pathog.* **13**, e1006290 (2017).
32. S. R. Lockhart *et al.*, Simultaneous emergence of multidrug-resistant *Candida auris* on 3 continents confirmed by whole-genome sequencing and epidemiological analyses. *Clin. Infect. Dis.* **64**, 134–140 (2017).
33. M. M. Harriott, M. C. Noverr, Importance of *Candida*-bacterial polymicrobial biofilms in disease. *Trends Microbiol.* **19**, 557–563 (2011).
34. D. A. Hogan, R. Kolter, *Pseudomonas-Candida* interactions: An ecological role for virulence factors. *Science* **296**, 2229–2232 (2002).
35. M. E. Rodrigues, F. Gomes, C. F. Rodrigues, *Candida* spp./bacteria mixed biofilms. *J. Fungi (Basel)* **6**, E5 (2019).
36. M. B. Lohse, M. Gulati, A. D. Johnson, C. J. Nobile, Development and regulation of single- and multi-species *Candida albicans* biofilms. *Nat. Rev. Microbiol.* **16**, 19–31 (2018).
37. G. Brunetti *et al.*, Candida gut colonization, yeast species distribution, and biofilm production in *Clostridioides difficile* infected patients: A comparison between three populations in two different time periods. *Braz. J. Microbiol.* **52**, 1845–1852 (2021).
38. W. Santus, J. R. Devlin, J. Behnsen, Crossing kingdoms: How the mycobiota and fungal-bacterial interactions impact host health and disease. *Infect. Immun.* **89**, e00648-20 (2021).
39. P. C. Seed, The human mycobiome. *Cold Spring Harb. Perspect. Med.* **5**, a019810 (2014).
40. D. R. Andes *et al.*; TRANSNET Investigators, The epidemiology and outcomes of invasive *Candida* infections among organ transplant recipients in the United States: Results of the Transplant-Associated Infection Surveillance Network (TRANSNET). *Transpl. Infect. Dis.* **18**, 921–931 (2016).
41. P. G. Pappas *et al.*, Invasive fungal infections among organ transplant recipients: Results of the Transplant-Associated Infection Surveillance Network (TRANSNET). *Clin. Infect. Dis.* **50**, 1101–1111 (2010).
42. M. A. Pfaller *et al.*, Epidemiology and outcomes of invasive candidiasis due to non-*albicans* species of *Candida* in 2,496 patients: Data from the Prospective Antifungal Therapy (PATH) registry 2004-2008. *PLoS One* **9**, e101510 (2014).
43. R. Zarnowski *et al.*, Coordination of fungal biofilm development by extracellular vesicle cargo. *Nat. Commun.* **12**, 6235 (2021).
44. D. L. Oliveira *et al.*, Characterization of yeast extracellular vesicles: Evidence for the participation of different pathways of cellular traffic in vesicle biogenesis. *PLoS One* **5**, e11113 (2010).
45. E. Dominguez *et al.*, Conservation and divergence in the *Candida* species biofilm matrix Mannan-Glucan complex structure, function, and genetic control. *MBio* **9**, e00451-18 (2018).
46. K. F. Mitchell *et al.*, Role of matrix β-1,3 glucan in antifungal resistance of non-*albicans Candida* biofilms. *Antimicrob. Agents Chemother.* **57**, 1918–1920 (2013).
47. G. Butler *et al.*, Evolution of pathogenicity and sexual reproduction in eight *Candida* genomes. *Nature* **459**, 657–662 (2009).
48. H. T. Taff *et al.*, A *Candida* biofilm-induced pathway for matrix glucan delivery: Implications for drug resistance. *PLoS Pathog.* **8**, e1002848 (2012).
49. K. F. Mitchell *et al.*, Community participation in biofilm matrix assembly and function. *Proc. Natl. Acad. Sci. U.S.A.* **112**, 4092–4097 (2015).
50. R. Zarnowski *et al.*, Novel entries in a fungal biofilm matrix encyclopedia. *MBio* **5**, e01333-14 (2014).
51. D. Andes *et al.*, Development and characterization of an in vivo central venous catheter *Candida albicans* biofilm model. *Infect. Immun.* **72**, 6023–6031 (2004).
52. K. Koeppen *et al.*, Let-7b-5p in vesicles secreted by human airway cells reduces biofilm formation and increases antibiotic sensitivity of *P. aeruginosa*. *Proc. Natl. Acad. Sci. U.S.A.* **118**, e2105370118 (2021).
53. T. Juan, M. Fürthauer, Biogenesis and function of ESCRT-dependent extracellular vesicles. *Semin. Cell Dev. Biol.* **74**, 66–77 (2018).
54. D. Zamith-Miranda *et al.*, Comparative molecular and immunoregulatory analysis of extracellular vesicles from *Candida albicans* and *Candida auris*. *mSystems* **6**, e0082221 (2021).
55. K. Kulig *et al.*, Insight into the properties and immunoregulatory effect of extracellular vesicles produced by *Candida glabrata*, *Candida parapsilosis*, and *Candida tropicalis* biofilms. *Front. Cell. Infect. Microbiol.* **12**, 879237 (2022).
56. A. A. Cleveland *et al.*, Changes in incidence and antifungal drug resistance in candidemia: Results from population-based laboratory surveillance in Atlanta and Baltimore, 2008-2011. *Clin. Infect. Dis.* **55**, 1352–1361 (2012).
57. N. A. Chow *et al.*, Tracing the evolutionary history and global expansion of *Candida auris* using population genomic analyses. *MBio* **11**, e03364-19 (2020).
58. J. Lötvall *et al.*, Minimal experimental requirements for definition of extracellular vesicles and their functions: A position statement from the International Society for Extracellular Vesicles. *J. Extracell. Vesicles* **3**, 26913 (2014).
59. J. E. Nett, A. J. Lepak, K. Marchillo, D. R. Andes, Time course global gene expression analysis of an in vivo *Candida* biofilm. *J. Infect. Dis.* **200**, 307–313 (2009).
60. J. P. Martínez *et al.*, Null mutants of *Candida albicans* for cell-wall-related genes form fragile biofilms that display an almost identical extracellular matrix proteome. *FEMS Yeast Res.* **16**, fow075 (2016).
61. S. García-Sánchez *et al.*, *Candida albicans* biofilms: A developmental state associated with specific and stable gene expression patterns. *Eukaryot. Cell* **3**, 536–545 (2004).
62. C. J. Nobile *et al.*, A recently evolved transcriptional network controls biofilm development in *Candida albicans*. *Cell* **148**, 126–138 (2012).
63. L. C. Dutton *et al.*, O-mannosylation in *Candida albicans* enables development of interkingdom biofilm communities. *MBio* **5**, e00911 (2014).
64. J. E. Nett, H. Sanchez, M. T. Cain, K. M. Ross, D. R. Andes, Interface of *Candida albicans* biofilm matrix-associated drug resistance and cell wall integrity regulation. *Eukaryot. Cell* **10**, 1660–1669 (2011).
65. R. Mancuso *et al.*, Functions of *Candida albicans* cell wall glycosidases *Dfg5p* and *Dcw1p* in biofilm formation and HOG MAPK pathway. *PeerJ* **6**, e5685 (2018).
66. C. J. Nobile *et al.*, Complementary adhesin function in *C. albicans* biofilm formation. *Curr. Biol.* **18**, 1017–1024 (2008).
67. E. G. Dominguez *et al.*, Conserved role for biofilm matrix polysaccharides in *Candida auris* drug resistance. *MSphere* **4**, e00680-18 (2019).
68. A. Mencher *et al.*, Proteomic characterization of extracellular vesicles produced by several wine yeast species. *Microb. Biotechnol.* **13**, 1581–1596 (2020).
69. M. Zhao *et al.*, Turbinmicin inhibits *Candida* biofilm growth by disrupting fungal vesicle-mediated trafficking. *J. Clin. Invest.* **131**, 145123 (2021).
70. D. L. Oliveira *et al.*, Extracellular vesicles from *Cryptococcus neoformans* modulate macrophage functions. *Infect. Immun.* **78**, 1601–1609 (2010).
71. E. F. Kong *et al.*, Commensal protection of *Staphylococcus aureus* against antimicrobials by *Candida albicans* biofilm matrix. *MBio* **7**, e01365-16 (2016).
72. D. Kim *et al.*, Bacterial-derived exopolysaccharides enhance antifungal drug tolerance in a cross-kingdom oral biofilm. *ISME J.* **12**, 1427–1442 (2018).
73. C. A. Kumamoto, M. S. Gresnigt, B. Hube, The gut, the bad and the harmless: *Candida albicans* as a commensal and opportunistic pathogen in the intestine. *Curr. Opin. Microbiol.* **56**, 7–15 (2020).
74. B. A. Peters, J. Wu, R. B. Hayes, J. Ahn, The oral fungal mycobiome: Characteristics and relation to periodontitis in a pilot study. *BMC Microbiol.* **17**, 157 (2017).
75. J. A. Romo, C. A. Kumamoto, On commensalism of *Candida*. *J. Fungi (Basel)* **6**, E16 (2020).
76. C. Ding *et al.*, Conserved and divergent roles of Bcr1 and CFEM proteins in *Candida parapsilosis* and *Candida albicans*. *PLoS One* **6**, e28151 (2011).
77. E. Mancera *et al.*, Evolution of the complex transcription network controlling biofilm formation in *Candida* species. *eLife* **10**, 10 (2021).
78. G. E. Moore, R. E. Gerner, H. A. Franklin, Culture of normal human leukocytes. *JAMA* **199**, 519–524 (1967).
79. E. Mancera, A. M. Porman, C. A. Cuomo, R. J. Bennett, A. D. Johnson, Finding a missing gene: EFG1 regulates morphogenesis in *Candida tropicalis*. *G3 (Bethesda)* **5**, 849–856 (2015).
80. L. M. Holland *et al.*, Comparative phenotypic analysis of the major fungal pathogens *Candida parapsilosis* and *Candida albicans*. *PLoS Pathog.* **10**, e1004365 (2014).
81. F. Istel, T. Schwarzmüller, M. Tscherner, K. Kuchler, Genetic transformation of *Candida glabrata* by electroporation. *Bio Protoc.* **5**, e1528 (2015).
82. R. M. Horton, H. D. Hunt, S. N. Ho, J. K. Pullen, L. R. Pease, Engineering hybrid genes without the use of restriction enzymes: Gene splicing by overlap extension. *Gene* **77**, 61–68 (1989).

83. R. Zarnowski, H. Sanchez, D. R. Andes, Large-scale production and isolation of *Candida* biofilm extracellular matrix. *Nat. Protoc.* **11**, 2320–2327 (2016).
84. J. E. Nett, M. T. Cain, K. Crawford, D. R. Andes, Optimizing a *Candida* biofilm microtiter plate model for measurement of antifungal susceptibility by tetrazolium salt assay. *J. Clin. Microbiol.* **49**, 1426–1433 (2011).
85. P. Shannon *et al.*, Cytoscape: A software environment for integrated models of biomolecular interaction networks. *Genome Res.* **13**, 2498–2504 (2003).
86. A. Jaromin *et al.*, Liposomal formulation of DIMIQ, potential antitumor indolo[2,3-b]quinoline agent and its cytotoxicity on hepatoma Morris 5123 cells. *Drug Deliv.* **15**, 49–56 (2008).
87. C. Gardiner, Y. J. Ferreira, R. A. Dragovic, C. W. Redman, I. L. Sargent, Extracellular vesicle sizing and enumeration by nanoparticle tracking analysis. *J. Extracell. Vesicles* **2**, 2 (2013).
88. S. E. Martin, J. Shabanowitz, D. F. Hunt, J. A. Marto, Subfemtomole MS and MS/MS peptide sequence analysis using nano-HPLC micro-ESI fourier transform ion cyclotron resonance mass spectrometry. *Anal. Chem.* **72**, 4266–4274 (2000).
89. D. N. Perkins, D. J. Pappin, D. M. Creasy, J. S. Cottrell, Probability-based protein identification by searching sequence databases using mass spectrometry data. *Electrophoresis* **20**, 3551–3567 (1999).
90. A. Keller *et al.*, Experimental protein mixture for validating tandem mass spectral analysis. *OMICS* **6**, 207–212 (2002).
91. S. Babicki *et al.*, Heatmapper: Web-enabled heat mapping for all. *Nucleic Acids Res.* **44** (W1), W147–W153 (2016).
92. Y. Perez-Riverol *et al.*, The PRIDE database and related tools and resources in 2019: Improving support for quantification data. *Nucleic Acids Res.* **47** (D1), D442–D450 (2019).
93. G. Sabat, D. Andes, Vesicle proteomics during fungal biofilm development in Candida. ProteomeXchange. http://proteomecentral.proteomexchange.org/cgi/GetDataset?ID=PXD035068. Deposited 4 July 2022.
94. M. Kanehisa, S. Goto, KEGG: Kyoto encyclopedia of genes and genomes. *Nucleic Acids Res.* **28**, 27–30 (2000).
95. M. Kanehisa, Y. Sato, M. Kawashima, KEGG mapping tools for uncovering hidden features in biological data. *Protein Sci.* **31**, 47–53 (2022).
96. M. S. Skrzypek *et al.*, The Candida Genome Database (CGD): Incorporation of Assembly 22, systematic identifiers and visualization of high throughput sequencing data. *Nucleic Acids Res.* **45** (D1), D592–D596 (2017).
97. J. F. S. Bernhardt, M. Hecker, J. Siebourg, "Visualizing gene expression data via Voronoi treemaps" in *Sixth International Symposium on Voronoi diagrams* (IEEE, 2009).
98. R. J. Henry, A. B. Blakeney, P. J. Harris, B. A. Stone, Detection of neutral and aminosugars from glycoproteins and polysaccharides as their alditol acetates. *J. Chromatogr. A* **256**, 419–427 (1983).